Periodic and rational solutions of the reduced Maxwell-Bloch equations

Jiao Wei[a], Xin Wang[a,b], Xianguo Geng[a]

[a]*School of Mathematics and Statistics, Zhengzhou University, 100 Kexue Road, Zhengzhou, Henan, 450001, China*

[b]*College of Science, Zhongyuan University of Technology, Zhengzhou, 450007, China*

Abstract

We investigate the reduced Maxwell-Bloch (RMB) equations which describe the propagation of short optical pulses in dielectric materials with resonant non-degenerate transitions. The general Nth-order periodic solutions are provided by means of the Darboux transformation, and from two different limiting cases of the obtained general periodic solutions, the Nth-order degenerate periodic and Nth-order rational solutions containing several free parameters with compact determinant representations are derived, respectively. Explicit expressions of these solutions from first to second order are presented. Typical nonlinear wave patterns for the four components of the RMB equations such as single-peak, double-peak-double-dip, double-peak and single-dip structures in the second-order rational solutions are shown. This kind of the rational solutions correspond to rogue waves in the reduced Maxwell-Bloch equations.

Keywords: Periodic solution; rational solution; Darboux transformation; reduced Maxwell-Bloch equations

1. Introduction

The associated reduced Maxwell-Bloch (RMB) equations play a fundamental role to describe wave phenomena in nonlinear optics related to self-induced transparency [1]. In dimensionless form, as

$$u_x = -\mu v, \tag{1a}$$

$$v_x = Ew + \mu u, \tag{1b}$$

$$w_x = -Ev, \tag{1c}$$

$$E_t = -v, \tag{1d}$$

with $E(x,t)$ the electric field, $u(x,t)$ atomic dipole, $v(x,t)$ phase information and $w(x,t)$ the atomic inversion. The integrability such as the Painlevé test and Lie-algebra-valued differential forms of the RMB equations have been investigated in Refs. [2, 3], and the explicit N-soliton solutions of the RMB equations have been respectively studied by the inverse scattering transform, Hirota bilinear technique and Darboux transformation (DT) during the past few decades [4–8].

Recently, it is well known that the generation of unexpectedly huge waves (termed as "rogue waves") has received widespread attention in quite a lot of researches including oceanography, optical fields, Bose-Einstein condensates, plasma physics, etc. [9–12]. The straightforward description of a single rogue wave in mathematics is the Peregrine soliton [13], a special solution of

---

the nonlinear Schrödinger (NLS) equation, which is a combination of the second-order rational polynomials and exponential function, and simulates the evolution of a wave of large amplitude that is localized in both space and time. More recently, beyond the NLS equation and its relevant physical systems [14–21], explicit periodic solutions, rational solutions and the generation of rogue waves in the modified Korteweg-de Vries (mKdV) equation have been studied by Chowdury, Slunyaev and He et al. [22–24]. As is pointed out by them, the existences of periodic and rational solutions in the mKdV equation reveal that breather and rogue wave phenomena are not confined to the deep ocean, and rogue wave phenomena governed by the mKdV equation present quite different descriptions in hydrodynamics from that related to the NLS equation.

In this paper, we demonstrate that Eq. (1) can also possess periodic and rational solutions like the mKdV equation, which will be helpful to understand the complicated rogue wave phenomena in nonlinear optics governed by the RMB equations. We present the general Nth-order periodic solutions on a finite constant background by using the classical DT with N eigenvalues that are different from each other [25–28]. Then, by taking advantage of the limit approach, namely the generalized DT [29–36], the Nth-order degenerate periodic and Nth-order rational solutions in the compact determinant representations can be respectively derived from two kinds of limiting cases of the general periodic solutions. As an application, explicit periodic, degenerate periodic and rational solutions up to second order are presented. We hereby show that the doubly-periodic lattice-like structure, and the single periodic- peaks or dips on a periodic wave background structure can exist in the second-order periodic and degenerate periodic solutions, respectively. Particularly, we demonstrate that, the second-order rational solutions for the four components E, v, w and u in Eq. (1) can provide distinctive patterns as a result of the collisions of a fixed number of dark and bright solitons, namely, the single-peak, double-peak-double-dip, double-peak and single-dip structures, respectively. Further, it is computed that the maximum amplitudes of the rational solutions from first to fourth order for the electric field E are the same as that of rogue waves from first to fourth order for the NLS equation [29]. Finally, it is confirmed that the free parameters can produce an important "differential shift"[22] effect on the peaks or dips with maximum or minimum amplitudes in the rational solutions.

The present paper is constructed as follows. In section 2, the general Nth-order periodic solutions are given by utilizing the classical DT. In sections 3 and 4, the Nth-order rational and Nth-order degenerate periodic solutions are derived through two different limit approaches, respectively. Explicit expressions of these obtained solutions from first to second order are presented, and some interesting wave patterns are shown. The last section is the conclusion of this paper.

2. Periodic solutions

For our studies, we begin with the Lax pair of Eq. (1) which can be given through the Ablowitz-Kaup-Newell-Segur (AKNS) technique [37–40]:

$$\Phi_x = U\Phi, U = \begin{pmatrix} -i\eta & -\dfrac{1}{2}E \\ \dfrac{1}{2}E & i\eta \end{pmatrix}, \tag{2}$$

$$\Phi_t = V\Phi, V = \frac{1}{4\eta^2 - \mu^2} \begin{pmatrix} -i\eta w & -i\eta v + \dfrac{1}{2}\mu u \\ -i\eta v - \dfrac{1}{2}\mu u & i\eta w \end{pmatrix}. \tag{3}$$

The compatibility condition $U_t - V_x + UV - VU = 0$ can directly give rise to Eq. (1).

Next, in order to obtain periodic solutions from the classical DT, we choose the following constant seeding solutions

$$E[0] = e_0, v[0] = 0, w[0] = -\frac{\mu u_0}{e_0}, u[0] = u_0. \tag{4}$$

By substituting the above solution into the linear system (2) and (3), and setting the eigenvalue $\eta = ie_0(1/2 + \epsilon^2)$ with ϵ being the pure imaginary small parameter such that $|\epsilon| < 1$, we have the following solution

$$\Phi(\epsilon) = \begin{pmatrix} \psi \\ \varphi \end{pmatrix} = \begin{pmatrix} C_1 e^A - C_2 e^{-A} \\ C_2 e^A - C_1 e^{-A} \end{pmatrix}, \tag{5}$$

where

$$C_1 = \frac{(1 + 2\epsilon^2 + 2\epsilon\sqrt{1 + \epsilon^2})^{\frac{1}{2}}}{2\epsilon\sqrt{1 + \epsilon^2}}, C_2 = \frac{(1 + 2\epsilon^2 - 2\epsilon\sqrt{1 + \epsilon^2})^{\frac{1}{2}}}{2\epsilon\sqrt{1 + \epsilon^2}},$$

and

$$A = e_0\epsilon\sqrt{1 + \epsilon^2} \left[x + \frac{\mu u_0}{e_0(4e_0^2\epsilon^4 + 4e_0^2\epsilon^2 + e_0^2 + \mu^2)} t \right].$$

After that, by letting $\Phi_j = (\psi_j, \varphi_j)^T = \Phi(\epsilon)|_{\epsilon=\epsilon_j}$ $(j = 1, 2, \cdots, N)$ be N special solutions of the linear system (2) and (3) with the constant seeding solutions (4) and $\eta_j = ie_0(1/2 + \epsilon_j^2)$, here $\epsilon_i \neq \epsilon_j$ for $i \neq j$. Thus, we can obtain the general Nth-order periodic solutions via the classical DT, viz.

$$E[N] = e_0 - 4i\frac{\det(M_1)}{\det(M)}, \tag{6}$$

$$v[N] = 4i\frac{\partial}{\partial t}\frac{\det(M_1)}{\det(M)}, \tag{7}$$

$$w[N] = -\frac{\mu u_0}{e_0} + 4i\frac{\partial}{\partial t}\frac{\det(M_2)}{\det(M)}, \tag{8}$$

and

$$u[N] = u_0 + \frac{4i}{\mu}\left[\frac{\partial^2}{\partial x\partial t}\frac{\det(M_1)}{\det(M)} - e_0\frac{\partial}{\partial t}\frac{\det(M_2)}{\det(M)} - \frac{\mu u_0}{e_0}\frac{\det(M_1)}{\det(M)} + 4i\frac{\det(M_1)}{\det(M)}\frac{\partial}{\partial t}\frac{\det(M_2)}{\det(M)} \right], \tag{9}$$

where

$$M = \begin{pmatrix} M_{11} & M_{12} & \cdots & M_{1N} \\ M_{21} & M_{22} & \cdots & M_{2N} \\ \vdots & \vdots & \ddots & \vdots \\ M_{N1} & M_{N2} & \cdots & M_{NN} \end{pmatrix},$$

$$M_1 = \begin{pmatrix} M_{11} & M_{12} & \cdots & M_{1N} & \varphi_1 \\ M_{21} & M_{22} & \cdots & M_{2N} & \varphi_2 \\ \vdots & \vdots & \ddots & \vdots & \vdots \\ M_{N1} & M_{N2} & \cdots & M_{NN} & \varphi_N \\ \psi_1 & \psi_2 & \cdots & \psi_N & 0 \end{pmatrix},$$

$$M_2 = \begin{pmatrix} M_{11} & M_{12} & \cdots & M_{1N} & \psi_1 \\ M_{21} & M_{22} & \cdots & M_{2N} & \psi_2 \\ \vdots & \vdots & \ddots & \vdots\vdots & \\ M_{N1} & M_{N2} & \cdots & M_{NN} & \psi_N \\ \psi_1 & \psi_2 & \cdots & \psi_N & 0 \end{pmatrix},$$

with

$$M_{ij} = \frac{\psi_j \psi_i + \varphi_j \varphi_i}{i e_0 (1 + \epsilon_j^2 + \epsilon_i^2)}, 1 \le i, j \le N.$$

At this point, by following the formulas (6)-(9) with $N = 1$, we can present the first-order periodic solutions

$$E[1]_p = e_0 \left[1 - 2 \frac{(2\kappa_1^2 - 1) + \cos(2\rho_1)}{1/(2\kappa_1^2 - 1) + \cos(2\rho_1)} \right], \tag{10}$$

$$v[1]_p = -2e_0 \frac{\partial}{\partial t} \left[\frac{(2\kappa_1^2 - 1) + \cos(2\rho_1)}{1/(2\kappa_1^2 - 1) + \cos(2\rho_1)} \right], \tag{11}$$

$$w[1]_p = -\frac{\mu u_0}{e_0} + 2e_0 \frac{\partial}{\partial t} \left[\frac{2\kappa_1 \sqrt{1 - \kappa_1^2} \sin(2\rho_1) + (2\kappa_1^2 - 1)\cos(2\rho_1) + 1}{1/(2\kappa_1^2 - 1) + \cos(2\rho_1)} \right], \tag{12}$$

and

$$u[1]_p = u_0 + \frac{4i}{\mu} \left[\frac{\partial^2}{\partial x \partial t} \frac{G_p^{[1]}}{F_p^{[1]}} - e_0 \frac{\partial}{\partial t} \frac{H_p^{[1]}}{F_p^{[1]}} - \frac{\mu u_0}{e_0} \frac{G_p^{[1]}}{F_p^{[1]}} + 4i \frac{G_p^{[1]}}{F_p^{[1]}} \frac{\partial}{\partial t} \frac{H_p^{[1]}}{F_p^{[1]}} \right], \tag{13}$$

where $\epsilon_1 = i\kappa_1$ with κ_1 being a real small parameter and satisfying $|\kappa_1| < 1$,

$$\rho_1 = e_0 \kappa_1 \sqrt{1 - \kappa_1^2} \left[x + \frac{\mu u_0}{e_0 (4e_0^2 \kappa_1^4 - 4e_0^2 \kappa_1^2 + e_0^2 + \mu^2)} t \right],$$

$$F_p^{[1]} = \frac{2\kappa_1^2 \cos(2\rho_1) - \cos(2\rho_1) + 1}{ie_0 \kappa_1^2 (2\kappa_1^2 - 1)(\kappa_1^2 - 1)}, G_p^{[1]} = -\frac{1}{2} \frac{[2\kappa_1^2 + \cos(2\rho_1) - 1]}{\kappa_1^2 (\kappa_1^2 - 1)},$$

$$H_p^{[1]} = \frac{1}{2} \frac{[2\kappa_1 \sqrt{1 - \kappa_1^2} \sin(2\rho_1) + 2\kappa_1^2 \cos(2\rho_1) - \cos(2\rho_1) + 1]}{\kappa_1^2 (\kappa_1^2 - 1)}.$$

The first-order periodic solutions (10)-(13) are shown in Fig. 1. It is seen that these solutions are periodic in both x and t and maintain constant amplitudes. The maximum amplitudes of the components E, v, w and u are 2, 0.88, 0.20 and -0.59, respectively.

For $N = 2$ in the formulas (6)-(9), the second-order periodic solutions can be worked out as

$$E[2]_p = e_0 - 4i \frac{G_p^{[2]}}{F_p^{[2]}}, \tag{14}$$

$$v[2]_p = 4i \frac{\partial}{\partial t} \frac{G_p^{[2]}}{F_p^{[2]}}, \tag{15}$$

$$w[2]_p = -\frac{\mu u_0}{e_0} + 4i \frac{\partial}{\partial t} \frac{H_p^{[2]}}{F_p^{[2]}}, \tag{16}$$

and

$$u[2]_p = u_0 + \frac{4i}{\mu} \left(\frac{\partial^2}{\partial x \partial t} \frac{G_p^{[2]}}{F_p^{[2]}} - e_0 \frac{\partial}{\partial t} \frac{H_p^{[2]}}{F_p^{[2]}} - \frac{\mu u_0}{e_0} \frac{G_p^{[2]}}{F_p^{[2]}} + 4i \frac{G_p^{[2]}}{F_p^{[2]}} \frac{\partial}{\partial t} \frac{H_p^{[2]}}{F_p^{[2]}} \right), \tag{17}$$

where

$$F_p^{[2]} = F_{11}F_{22} - F_{12}F_{21}, G_p^{[2]} = -F_{11}c_2d_2 + F_{12}c_1d_2 + F_{21}c_2d_1 - F_{22}c_1d_1,$$
$$H_p^{[2]} = -F_{11}c_2^2 + F_{12}c_1c_2 + F_{21}c_1c_2 - F_{22}c_1^2,$$

with

$$F_{11} = \frac{2\kappa_1^2 \cos(2\rho_1) - \cos(2\rho_1) + 1}{ie_0\kappa_1^2(2\kappa_1^2 - 1)(\kappa_1^2 - 1)}, F_{22} = \frac{2\kappa_2^2 \cos(2\rho_2) - \cos(2\rho_2) + 1}{ie_0\kappa_2^2(2\kappa_2^2 - 1)(\kappa_2^2 - 1)},$$

$$F_{12} = F_{21} = \frac{2i[\sqrt{1-\kappa_1^2}\sqrt{1-\kappa_2^2}\sin(\rho_1)\sin(\rho_2) + \kappa_1\kappa_2\cos(\rho_1)\cos(\rho_2)]}{e_0\kappa_1\kappa_2(\kappa_1^2 + \kappa_2^2 - 1)\sqrt{1-\kappa_1^2}\sqrt{1-\kappa_2^2}},$$

$$c_1 = \frac{\sqrt{1-\kappa_1^2}\sin(\rho_1) + \kappa_1\cos(\rho_1)}{\kappa_1\sqrt{1-\kappa_1^2}}, c_2 = \frac{\sqrt{1-\kappa_2^2}\sin(\rho_2) + \kappa_2\cos(\rho_2)}{\kappa_2\sqrt{1-\kappa_2^2}},$$

$$d_1 = \frac{\sqrt{1-\kappa_1^2}\sin(\rho_1) - \kappa_1\cos(\rho_1)}{\kappa_1\sqrt{1-\kappa_1^2}}, d_2 = \frac{\sqrt{1-\kappa_2^2}\sin(\rho_2) - \kappa_2\cos(\rho_2)}{\kappa_2\sqrt{1-\kappa_2^2}},$$

$$\rho_j = e_0\kappa_j\sqrt{1-\kappa_j^2}\left[x + \frac{\mu u_0}{e_0(4e_0^2\kappa_j^4 - 4e_0^2\kappa_j^2 + e_0^2 + \mu^2)}t\right], j = 1, 2.$$

Here we take $\epsilon_j = i\kappa_j$ with κ_j being a real parameter and yielding $|\kappa_j| < 1$.

In this circumstance, the doubly-periodic lattice-like structures can be displayed, see Fig. 2. The maximum amplitudes of the peaks for the components E, v and w are 3.75, 1.41 and 1.41. While for the component u, the doubly-periodic lattice-like dip structure appears, and the minimum amplitude of the dips is 0.17.

3. Degenerate periodic solutions

In this section, we derive the degenerate periodic solutions of Eq. (1) from one limiting case of the general Nth-order periodic solutions (6)-(9). To this end, we give the following Taylor series

$$\psi(\epsilon) = \sum_{i=0}^{N-1}\psi_1^{[i]}(\epsilon - \epsilon_1)^i + \mathcal{O}\left((\epsilon - \epsilon_1)^N\right), \varphi(\epsilon) = \sum_{i=0}^{N-1}\varphi_1^{[i]}(\epsilon - \epsilon_1)^i + \mathcal{O}\left((\epsilon - \epsilon_1)^N\right), \quad (18)$$

and define

$$\frac{\psi(\epsilon^*)\psi(\epsilon) + \varphi(\epsilon^*)\varphi(\epsilon)}{ie_0(1 + \epsilon^2 + \epsilon^{*2})} = \sum_{i,j=1}^{N} P^{[i,j]}(\epsilon - \epsilon_1)^{j-1}(\epsilon^* - \epsilon_1)^{i-1} + \mathcal{O}\left((\epsilon - \epsilon_1)^N(\epsilon^* - \epsilon_1)^N\right), \quad (19)$$

where

$$\psi_1^{[i]} = \lim_{\epsilon \to \epsilon_1}\frac{1}{i!}\frac{\partial^i\psi_1}{\partial\epsilon^i}, \varphi_1^{[i]} = \lim_{\epsilon \to \epsilon_1}\frac{1}{i!}\frac{\partial^i\varphi_1}{\partial\epsilon^i},$$

and

$$P^{[i,j]} = \frac{1}{(i-1)!(j-1)!}\frac{\partial^{i+j-2}}{\partial\epsilon^{j-1}\partial\epsilon^{*i-1}}\frac{\psi(\epsilon^*)\psi(\epsilon) + \varphi(\epsilon^*)\varphi(\epsilon)}{ie_0(1 + \epsilon^2 + \epsilon^{*2})}\Bigg|_{\epsilon,\epsilon^* \to \epsilon_1}.$$

Here ϵ^* is the other introduced complex small parameter, and ϵ_1 is a pure imaginary small parameter such that $\epsilon_1 \neq 0$. At this time, the Nth-order degenerate periodic solutions can be expressed

as

$$E[N] = e_0 - 4i\frac{\det(P_1)}{\det(P)}, \tag{20}$$

$$v[N] = 4i\frac{\partial}{\partial t}\frac{\det(P_1)}{\det(P)}, \tag{21}$$

$$w[N] = -\frac{\mu u_0}{e_0} + 4i\frac{\partial}{\partial t}\frac{\det(P_2)}{\det(P)}, \tag{22}$$

and

$$u[N] = u_0 + \frac{4i}{\mu}\left[\frac{\partial^2}{\partial x \partial t}\frac{\det(P_1)}{\det(P)} - e_0\frac{\partial}{\partial t}\frac{\det(P_2)}{\det(P)} - \frac{\mu u_0}{e_0}\frac{\det(P_1)}{\det(P)} + 4i\frac{\det(P_1)}{\det(P)}\frac{\partial}{\partial t}\frac{\det(P_2)}{\det(P)}\right], \tag{23}$$

where

$$P = \begin{pmatrix} P^{[11]} & P^{[12]} & \cdots & P^{[1N]} \\ P^{[21]} & P^{[22]} & \cdots & P^{[2N]} \\ \vdots & \vdots & \ddots & \vdots \\ P^{[N1]} & P^{[N2]} & \cdots & P^{[NN]} \end{pmatrix},$$

$$P_1 = \begin{pmatrix} P^{[11]} & P^{[12]} & \cdots & P^{[1N]} & \varphi_1^{[0]} \\ P^{[21]} & P^{[22]} & \cdots & P^{[2N]} & \varphi_1^{[1]} \\ \vdots & \vdots & \ddots & \vdots\vdots & \vdots \\ P^{[N1]} & P^{[N2]} & \cdots & P^{[NN]} & \varphi_1^{[N-1]} \\ \psi_1^{[0]} & \psi_1^{[1]} & \cdots & \psi_1^{[N-1]} & 0 \end{pmatrix},$$

$$P_2 = \begin{pmatrix} P^{[11]} & P^{[12]} & \cdots & P^{[1N]} & \psi_1^{[0]} \\ P^{[21]} & P^{[22]} & \cdots & P^{[2N]} & \psi_1^{[1]} \\ \vdots & \vdots & \ddots & \vdots\vdots & \vdots \\ P^{[N1]} & P^{[N2]} & \cdots & P^{[NN]} & \psi_1^{[N-1]} \\ \psi_1^{[0]} & \psi_1^{[1]} & \cdots & \psi_1^{[N-1]} & 0 \end{pmatrix}.$$

Explicitly, for simplicity, we now choose a special small parameter of $\epsilon_1 = 1/2i$, then the degenerate periodic solutions take the form as

$$E[2]_d = e_0 - 4i\frac{G_d^{[2]}}{F_d^{[2]}}, \tag{24}$$

$$v[2]_d = 4i\frac{\partial}{\partial t}\frac{G_d^{[2]}}{F_d^{[2]}}, \tag{25}$$

$$w[2]_d = -\frac{\mu u_0}{e_0} + 4i\frac{\partial}{\partial t}\frac{H_d^{[2]}}{F_d^{[2]}}, \tag{26}$$

and

$$u[2]_d = u_0 + \frac{4i}{\mu}\left(\frac{\partial^2}{\partial x \partial t}\frac{G_d^{[2]}}{F_d^{[2]}} - e_0\frac{\partial}{\partial t}\frac{H_d^{[2]}}{F_d^{[2]}} - \frac{\mu u_0}{e_0}\frac{G_d^{[2]}}{F_d^{[2]}} + 4i\frac{G_d^{[2]}}{F_d^{[2]}}\frac{\partial}{\partial t}\frac{H_d^{[2]}}{F_d^{[2]}}\right), \tag{27}$$

where the explicit expressions of the mixed functions containing rational polynomials and trigonometric functions are given in appendix A.

For $N = 1$, the degenerate periodic solutions in the above formulas are reduced to the first-order periodic solutions (10)-(13) given in the above section. For $N = 2$, the simplest nontrivial

degenerate periodic solutions can be shown, see Fig. 3. The patterns of these solutions for the components E, v and w consist of a single periodic- peaks on a periodic wave background, and the maximum amplitudes of the peaks are 3, 1.40 and 1.24, respectively. While for the component u, it is exhibited that a singe periodic- dips on a periodic wave background structure exists, and the minimum amplitude of the dips is -0.15.

4. Rational solutions

In this section, let us take a further look at the general periodic solutions by employing the limit approach of $\epsilon_1 \to 0$. We now adjust the expression A in (5) as

$$A = e_0 \epsilon \sqrt{1 + \epsilon^2} \left[x + \frac{\mu u_0}{e_0(4e_0^2 \epsilon^4 + 4e_0^2 \epsilon^2 + e_0^2 + \mu^2)} t + \sum_{i=1}^{N-1} s_i \epsilon^{2i} \right],$$

here s_i are $(N-1)$ new introduced complex free parameters. Accordingly, the Taylor series (18) and (19) can be rewritten as

$$\psi(\epsilon) = \sum_{i=0}^{N-1} \widehat{\psi_1^{[i]}} \epsilon^{2i} + \mathcal{O}\left(\epsilon^{2N}\right), \varphi(\epsilon) = \sum_{i=0}^{N-1} \widehat{\varphi_1^{[i]}} \epsilon^{2i} + \mathcal{O}\left(\epsilon^{2N}\right), \tag{28}$$

and

$$\frac{\psi(\epsilon^*)\psi(\epsilon) + \varphi(\epsilon^*)\varphi(\epsilon)}{ie_0(1 + \epsilon^2 + \epsilon^{*2})} = \sum_{i,j=1}^{N} Q^{[i,j]} \epsilon^{2(j-1)} \epsilon^{*2(i-1)} + \mathcal{O}\left((\epsilon\epsilon^*)^{2N}\right), \tag{29}$$

where

$$\widehat{\psi_1^{[i]}} = \lim_{\epsilon \to 0} \frac{1}{2i!} \frac{\partial^{2i} \psi_1}{\partial \epsilon^{2i}}, \widehat{\varphi_1^{[i]}} = \lim_{\epsilon \to 0} \frac{1}{2i!} \frac{\partial^{2i} \varphi_1}{\partial \epsilon^{2i}},$$

and

$$Q^{[i,j]} = \frac{1}{2(i-1)!2(j-1)!} \frac{\partial^{2(i+j-2)}}{\partial \epsilon^{2(j-1)} \partial \epsilon^{*2(i-1)}} \frac{\psi(\epsilon^*)\psi(\epsilon) + \varphi(\epsilon^*)\varphi(\epsilon)}{ie_0(1 + \epsilon^2 + \epsilon^{*2})} \Bigg|_{\epsilon, \epsilon^* \to 0}.$$

At present, we can put forward the Nth-order rational solution as

$$E[N] = e_0 - 4i \frac{\det(Q_1)}{\det(Q)}, \tag{30}$$

$$v[N] = 4i \frac{\partial}{\partial t} \frac{\det(Q_1)}{\det(Q)}, \tag{31}$$

$$w[N] = -\frac{\mu u_0}{e_0} + 4i \frac{\partial}{\partial t} \frac{\det(Q_2)}{\det(Q)}, \tag{32}$$

and

$$u[N] = u_0 + \frac{4i}{\mu} \left[\frac{\partial^2}{\partial x \partial t} \frac{\det(Q_1)}{\det(Q)} - e_0 \frac{\partial}{\partial t} \frac{\det(Q_2)}{\det(Q)} - \frac{\mu u_0}{e_0} \frac{\det(Q_1)}{\det(Q)} + 4i \frac{\det(Q_1)}{\det(Q)} \frac{\partial}{\partial t} \frac{\det(Q_2)}{\det(Q)} \right], \tag{33}$$

where

$$Q = \begin{pmatrix} Q^{[11]} & Q^{[12]} & \cdots & Q^{[1N]} \\ Q^{[21]} & Q^{[22]} & \cdots & Q^{[2N]} \\ \vdots & \vdots & \ddots & \vdots \\ Q^{[N1]} & Q^{[N2]} & \cdots & Q^{[NN]} \end{pmatrix},$$

$$Q_1 = \begin{pmatrix} Q^{[11]} & Q^{[12]} & \cdots & Q^{[1N]} & \widehat{\varphi_1^{[0]}} \\ Q^{[21]} & Q^{[22]} & \cdots & Q^{[2N]} & \widehat{\varphi_1^{[1]}} \\ \vdots & \vdots & \ddots & \vdots & \vdots \\ Q^{[N1]} & Q^{[N2]} & \cdots & Q^{[NN]} & \widehat{\varphi_1^{[N-1]}} \\ \widehat{\psi_1^{[0]}} & \widehat{\psi_1^{[1]}} & \cdots & \widehat{\psi_1^{[N-1]}} & 0 \end{pmatrix},$$

$$Q_2 = \begin{pmatrix} Q^{[11]} & Q^{[12]} & \cdots & Q^{[1N]} & \widehat{\psi_1^{[0]}} \\ Q^{[21]} & Q^{[22]} & \cdots & Q^{[2N]} & \widehat{\psi_1^{[1]}} \\ \vdots & \vdots & \ddots & \vdots & \vdots \\ Q^{[N1]} & Q^{[N2]} & \cdots & Q^{[NN]} & \widehat{\psi_1^{[N-1]}} \\ \widehat{\psi_1^{[0]}} & \widehat{\psi_1^{[1]}} & \cdots & \widehat{\psi_1^{[N-1]}} & 0 \end{pmatrix}.$$

With these formulas for $N = 1$, we can get the explicit first-order rational solutions, viz.

$$E[1]_r = -e_0 + \frac{4e_0(e_0^4 + 2e_0^2\mu^2 + \mu^4)}{F_r^{[1]}}, \tag{34}$$

$$v[1]_r = \frac{8e_0\mu u_0(e_0^2 + \mu^2)^2(e_0^3 x + e_0\mu^2 x + \mu u_0 t)}{F_r^{[1]2}}, \tag{35}$$

$$w[1]_r = -\frac{\mu u_0}{e_0} - \frac{4e_0\mu u_0(e_0^2 + \mu^2)H_r^{[1]}}{F_r^{[1]2}}, \tag{36}$$

$$u[1]_r = -u_0 + \frac{4\mu^2 u_0(e_0^2 + \mu^2)}{F_r^{[1]}}, \tag{37}$$

where

$$H_r^{[1]} = (e_0^3 x + e_0\mu^2 x + \mu u_0 t + e_0^2 + \mu^2)(e_0^3 x + e_0\mu^2 x + \mu u_0 t - e_0^2 - \mu^2),$$
$$F_r^{[1]} = e_0^6 x^2 + 2e_0^4\mu^2 x^2 + e_0^2\mu^4 x^2 + 2e_0^3\mu u_0 xt + 2e_0\mu^3 t u_0 x + \mu^2 t^2 u_0^2 + e_0^4 + 2e_0^2\mu^2 + \mu^4.$$

The above solutions correspond to the Peregrine soliton of the NLS equation [13]. Nevertheless, unlike the Peregrine soliton that is doubly localized, these solutions look more like the solitons on a finite constant background. For the component E, there is one ridge with maximum amplitude $3e_0$ on the temporal-spatial distribution, see Fig. 4(a). The critical line is given by

$$t = -\frac{e_0(e_0^2 + \mu^2)}{\mu u_0} x. \tag{38}$$

For the component v, it is displayed in Fig. 4(b) that, there are one ridge with maximum amplitude and one valley with minimum amplitude on the coordinate plane. The maximum and minimum

values of $v[1]$ are $\pm 3\sqrt{3}e_0\mu u_0/2(e_0^2 + \mu^2)$, and occur at

$$t = -\frac{e_0(e_0^2 + \mu^2)}{\mu u_0}x \pm \frac{\sqrt{3}(e_0^2 + \mu^2)}{3\mu u_0}.$$

Moreover, $w[1]$ is shown in Fig. 4(c), and there exist one ridge with maximum amplitude and two valleys with minimum amplitude on the temporal-spatial plane. The maximum value of $w[1]$ is $(3e_0^2 - \mu^2)\mu u_0/e_0(e_0^2 + \mu^2)$ and the critical line is defined by Eq. (38). While the minimum value of $w[1]$ is $-(3e_0^2 + 2\mu^2)\mu u_0/2e_0(e_0^2 + \mu^2)$ and is reached at

$$t = -\frac{e_0(e_0^2 + \mu^2)}{\mu u_0}x \pm \frac{\sqrt{3}(e_0^2 + \mu^2)}{\mu u_0}.$$

In succession, the maximum amplitude of $u[1]$ is $-(e_0^2 - 3\mu^2)u_0/(e_0^2 + \mu^2)$ and the critical line is defined by Eq. (38), see Fig. 4(d).

Additionally, it can be checked that

$$\int_{-\infty}^{\infty}(E[1]_r - E[1]_{r0})^2\mathrm{d}x = 8\pi\mathrm{sgn}(e_0)e_0,$$

$$\int_{-\infty}^{\infty}(v[1]_r - v[1]_{r0})^2\mathrm{d}x = \int_{-\infty}^{\infty}(w[1]_r - w[1]_{r0})^2\mathrm{d}x = \frac{4\pi\mu^2 u_0^2\mathrm{sgn}(e_0)e_0}{(e_0^2 + \mu^2)^2},$$

$$\int_{-\infty}^{\infty}(u[1]_r - u[1]_{r0})^2\mathrm{d}x = \frac{8\pi\mu^4 u_0^2\mathrm{sgn}(e_0)}{e_0(e_0^2 + \mu^2)^2},$$

where $E[1]_{r0}, v[1]_{r0}, w[1]_{r0}, w[1]_{r0} = \lim_{x\to\pm\infty} E[1]_r, v[1]_r, w[1]_r, u[1]_r$, which indicate that energies of the Peregrine pulses of the first-order rational solutions keep a constant.

Afterwards, by applying $N = 2$ in the formulas (30)-(33), we can present the second-order rational solutions

$$E[2]_r = e_0 - 4i\frac{G_r^{[2]}}{F_r^{[2]}}, \tag{39}$$

$$v[2]_r = 4i\frac{\partial}{\partial t}\frac{G_r^{[2]}}{F_r^{[2]}}, \tag{40}$$

$$w[2]_r = -\frac{\mu u_0}{e_0} + 4i\frac{\partial}{\partial t}\frac{H_r^{[2]}}{F_r^{[2]}}, \tag{41}$$

and

$$u[2]_r = u_0 + \frac{4i}{\mu}\left(\frac{\partial^2}{\partial x\partial t}\frac{G_r^{[2]}}{F_r^{[2]}} - e_0\frac{\partial}{\partial t}\frac{H_r^{[2]}}{F_r^{[2]}} - \frac{\mu u_0}{e_0}\frac{G_r^{[2]}}{F_r^{[2]}} + 4i\frac{G_r^{[2]}}{F_r^{[2]}}\frac{\partial}{\partial t}\frac{H_r^{[2]}}{F_r^{[2]}}\right), \tag{42}$$

where the polynomials are explicitly provided in appendix B.

Shown in Fig. 5 are the second-order rational solutions (39)-(42). It is exhibited that some typical nonlinear wave patterns can emerge and they are seemingly a result of the collisions of a fixed number of dark and bright solitons. For the component E, we can see the single-peak structure in Fig. 5(a). The maximum amplitude of $E[2]$ is 5 and is localized at $(0, 0)$, which coincides with the second-order fundamental rogue wave in the NLS equation [14, 29]. For the component v, it is interestingly found that the double-peak-double-dip structure can arise, see Fig. 5(b). We calculate that the maximum amplitude of $v[2]$ is 1.41 and occurs at $(0.05, 1.18)$

and $(0.94, -1.40)$, and the minimum amplitude of it is -1.41 and arrives at $(-0.05, -1.18)$ and $(-0.94, 1.40)$. Furthermore, the nonlinear wave in Fig. 5(c) for the component w is the double-peak structure, which has the maximum amplitude of 1.41 and reaches at the two points of $(0.27, -0.91)$ and $(-0.27, 0.91)$. More interestingly, it is worthwhile to emphasize that, for the component u in Fig. 5(d), the single-dip structure can be exhibited, which is quite different from the single-peak case for the component E and the relevant structure in the mKdV equation [22]. The minimum amplitude of $u[2]$ is 0.56 and is acquired at the original point. At the same time, we can see that in Fig. 6, the nonzero free parameter s_1 can produce an important shift effect on the peaks or dips along the wave trough in the second-order rational solutions. But, it does not affect the maximum or minimum amplitudes of these solutions.

For the higher-order cases, we only show the evolution plots of the third- and fourth-order rational solutions for the component E, and omit writing down the corresponding cumbersome expressions, see Figs. 7 and 8. We exhibit that the third-order rational solutions can be viewed as the collisions of a dark and two bright solitons, and the fourth-order rational solutions are likely the result of the collisions of two dark and two bright solitons. It is computed that when setting all of the free parameters s_i be zero, then the maximum amplitudes of the third- and fourth-order rational solutions are 7 and 9, respectively, which are the same as that of the third- and fourth-order rogue waves in the NLS equation [14, 29]. While when taking one of the free parameters be nonzero such as $s_1 \neq 0$, then the highest peaks in these higher-order rational solutions can also have a shift along the depressed wave trough. In this circumstance, unlike the second-order rational solutions, the maximum amplitudes of the higher-order solutions are changed due to the interactions among the multiple solitons. The maximum amplitudes of the highest peaks in Figs. 7(b) and 8(b) become 4.77 and 5.96, respectively.

5. Conclusion

In summary, we proposed the general Nth-order periodic, Nth-order degenerate periodic and Nth-order rational solutions with the compact determinant representations for the RMB equations, which serve as the fundamental model in nonlinear optics associated with self-induced transparency. The explicit first- and second-order periodic and rational solutions are presented. Some interesting nonlinear wave patterns described by the second-order periodic solution, the simplest degenerate periodic solutions, and especially the higher-order rational solutions are shown. Also, it is notable to remark that the limit approach using in this paper can be directly applied to the mKdV equation [22, 24], the variable-coefficient mKdV equation [41] and other mKdV-type equations. We hope our results given in this paper may be helpful to interpret the intricate rogue wave phenomena in nonlinear optics governed by the RMB equations.

Appendix A: mixed functions in Eqs. (24)-(27)

$$
\begin{aligned}
F_d^{[2]} = & -\frac{256}{27e_0^2(e_0^2 + 4\mu^4)^4}[-2352e_0^4\mu^2 u_0^2 t^2 - 2688e_0^2\mu^4 u_0^2 t^2 - 768\mu^6 u_0^2 t^2 - 168e_0^7\mu\, u_0 tx \\
& - 1440e_0^5\mu^3 u_0 tx - 3456e_0^3\mu^5 u_0 tx - 1536e_0\mu^7 u_0 tx - 3e_0^{10}x^2 - 48e_0^8\mu^2 x^2 - 288e_0^6\mu^4 x^2 \\
& - 768e_0^4\mu^6 x^2 - 768e_0^2\mu^8 x^2 + 16(e_0^2 + 4\mu^2)^4\cos(\omega)^4 + 80(e_0^2 + 4\mu^2)^4\cos(\omega)^2 \\
& + 16\sqrt{3}(28e_0^2\mu u_0 t + 16\mu^3 u_0 t + e_0^5 x + 8e_0^3\mu^2 x + 16e_0\mu^4 x)(e_0^2 + 4\mu^2)^2\sin(\omega)\cos(\omega) \\
& - 108e_0^8 - 1728e_0^6\mu^2 - 10368e_0^4\mu^4 - 27648e_0^2\mu^6 - 27648\mu^8],
\end{aligned}
$$

$$F_d^{[2]} = \frac{512i}{9e_0(e_0^2 + 4\mu^4)^4}[10(e_0^2 + 4\mu^2)^2\cos(\omega)^2 + \sqrt{3}(28e_0^2\mu u_0 t + 16\mu^3 u_0 t + e_0^5 x + 8e_0^3\mu^2 x$$
$$+ 16e_0\mu^4 x)\sin(\omega)\cos(\omega) - 9(e_0^2 + 4\mu^2)^2],$$

$$H_d^{[2]} = -\frac{256}{27e_0^2(e_0^2 + 4\mu^4)^4}[2352e_0^4\mu^2 u_0^2 t^2 + 2688e_0^2\mu^4 u_0^2 t^2 + 768\mu^6 u_0^2 t^2 + 1536e_0\mu^7 u_0 tx$$
$$+ 3456e_0^3\mu^5 u_0 tx + 168e_0^7\mu u_0 tx + 1440e_0^5\mu^3 u_0 tx + 288e_0^6\mu^4 x^2 + 768e_0^4\mu^6 x^2 + 768e_0^2\mu^8 x^2$$
$$+ 3e_0^{10}x^2 + 48e_0^8\mu^2 x^2 + 4608\mu^7 u_0 t + 504e_0^6\mu u_0 t + 4320e_0^4\mu^3 u_0 t + 10368e_0^2\mu^5 u_0 t$$
$$+ 288e_0^7\mu^2 x + 1728e_0^5\mu^4 x + 4608e_0^3\mu^6 x + 4608e_0\mu^8 x + 18e_0^9 x + 10368e_0^4\mu^4 + 27648e_0^2\mu^6$$
$$+ 16\sqrt{3}(e_0^2 + 4\mu^2)^4\sin(\omega)\cos(\omega)^3 - 8(e_0^2 + 4\mu^2)^2(84e_0^2\mu u_0 t + 48\mu^3 u_0 t + 3e_0^5 x$$
$$+ 24e_0^3\mu^2 x + 48e_0\mu^4 x + 10e_0^4 + 80e_0^2\mu^2 + 160\mu^4)\cos(\omega)^2 - 16(e_0^2 + 4\mu^2)^4\cos(\omega)^4$$
$$+ 1728e_0^6\mu^2 + 27648\mu^8 + 108e_0^8 - 8\sqrt{3}(56e_0^2\mu u_0 t + 32\mu^3 u_0 t + 2e_0^5 x + 16e_0^3\mu^2 x$$
$$+ 32e_0\mu^4 x - 3e_0^4 - 24e_0^2\mu^2 - 48\mu^4)(e_0^2 + 4\mu^2)^2\sin(\omega)\cos(\omega)],$$

in which $\omega = \sqrt{3}(e_0^3 x + 4e_0\mu^2 x + 4\mu u_0 t)/4(e_0^2 + 4\mu^2)$.

Appendix B: polynomials in Eqs. (39)-(42)

$$F_r^{[2]} = -\frac{4}{9e_0^2(e_0^2 + \mu^2)^6}[\mu^6 u_0^6 t^6 + 6e_0\mu^5 u_0^5(e_0^2 + \mu^2)t^5 x + e_0^6(e_0^2 + \mu^2)^6 x^6 + (15e_0^2\mu^4 u_0^4(e_0^2 + \mu^2)^2 x^2$$
$$+ 3\mu^4 u_0^4(9e_0^2 + \mu^2)(e_0^2 + \mu^2))t^4 + 3e_0^4(e_0^2 + \mu^2)^6 x^4 + (20e_0^3\mu^3 u_0^3(e_0^2 + \mu^2)^3 x^3$$
$$+ 12e_0\mu^3 u_0^3(7e_0^2 + \mu^2)(e_0^2 + \mu^2)^2 x - 6e_0\mu^3 s_1 u_0^3(e_0^2 + \mu^2)^3)t^3 - 6e_0^4 s_1(e_0^2 + \mu^2)^6 x^3$$
$$+ (15e_0^4\mu^2 u_0^2(e_0^2 + \mu^2)^4 x^4 + 18e_0^2\mu^2 u_0^2(5e_0^2 + \mu^2)(e_0^2 + \mu^2)^3 x^2 - 18e_0^2\mu^2 s_1 u_0^2(e_0^2$$
$$+ \mu^2)^4 x + 9\mu^2 u_0^2(11e_0^4 - 2e_0^2\mu^2 + 3\mu^4)(e_0^2 + \mu^2)^2)t^2 + 27e_0^2(e_0^2 + \mu^2)^6 x^2$$
$$+ (6e_0^5\mu u_0(e_0^2 + \mu^2)^5 x^5 + 12e_0^3\mu u_0(3e_0^2 + \mu^2)(e_0^2 + \mu^2)^4 x^3 - 18e_0^3\mu s_1 u_0(e_0^2$$
$$+ \mu^2)^5 x^2 - 18e_0\mu u_0(e_0^2 - 3\mu^2)(e_0^2 + \mu^2)^4 x - 18e_0\mu s_1 u_0(3e_0^2 - \mu^2)(e_0^2 + \mu^2)^4)t$$
$$+ 18e_0^2 s_1(e_0^2 + \mu^2)^6 x + (9(e_0^2 s_1^2 + 1))(e_0^2 + \mu^2)^6],$$

$$G_r^{[2]} = \frac{4i}{3e_0^2(e_0^2 + \mu^2)^6}[\mu^4 u_0^4 t^4 + 4e_0\mu^3 u_0^3(e_0^2 + \mu^2)t^3 x + e_0^4(e_0^2 + \mu^2)^4 x^4 + (6\mu^2 u_0^2 e_0^2(e_0^2 + \mu^2)^2 x^2$$
$$- 6\mu^2 u_0^2(3e_0^2 - \mu^2)(e_0^2 + \mu^2))t^2 + 6e_0^2(e_0^2 + \mu^2)^4 x^2 + (4e_0^3\mu u_0(e_0^2 + \mu^2)^3 x^3$$
$$+ 12u_0\mu e_0(e_0^2 - \mu^2)(e_0^2 + \mu^2)^2 x + 6e_0\mu s_1 u_0(e_0^2 + \mu^2)^3)t + 6e_0^2 s_1(e_0^2 + \mu^2)^4 x$$
$$- 3(e_0^2 + \mu^2)^4],$$

$$H_r^{[2]} = \frac{4i}{9e_0^2(e_0^2 + \mu^2)^6}[\mu^6 u_0^6 t^6 + e_0^6(e_0^2 + \mu^2)^6 x^6 + (6e_0\mu^5 u_0^5(e_0^2 + \mu^2)x + 3\mu^5 u_0^5(e_0^2 + \mu^2))t^5$$
$$+ 3e_0^5(e_0^2 + \mu^2)^6 x^5 + (15e_0^2\mu^4 u_0^4(e_0^2 + \mu^2)^2 x^2 + 15e_0\mu^4 u_0^4(e_0^2 + \mu^2)^2 x$$
$$+ 3\mu^4 u_0^4(9e_0^2 + \mu^2)(e_0^2 + \mu^2))t^4 + 3e_0^4(e_0^2 + \mu^2)^6 x^4 + (20e_0^3\mu^3 u_0^3(e_0^2$$
$$+ \mu^2)^3 x^3 + 30e_0^2\mu^3 u_0^3(e_0^2 + \mu^2)^3 x^2 + 12e_0\mu^3 u_0^3(7e_0^2 + \mu^2)(e_0^2 + \mu^2)^2 x$$
$$- 6\mu^3 u_0^3(e_0^2 + \mu^2)^2(e_0^3 s_1 + e_0\mu^2 s_1 - 7e_0^2 - \mu^2))t^3 - 6e_0^3(e_0^2 + \mu^2)^6(e_0 s_1 - 1)x^3$$
$$+ (15e_0^4\mu^2 u_0^2(e_0^2 + \mu^2)^4 x^4 + 30e_0^3\mu^2 u_0^2(e_0^2 + \mu^2)^4 x^3 + 18e_0^2\mu^2 u_0^2(5e_0^2$$
$$+ \mu^2)(e_0^2 + \mu^2)^3 x^2 - 18e_0\mu^2 u_0^2(e_0^2 + \mu^2)^3(e_0^3 s_1 + e_0\mu^2 s_1 - 5e_0^2 - \mu^2)x$$
$$- 9\mu^2 u_0^2(e_0^2 + \mu^2)^2(e_0^5 s_1 + 2e_0^3\mu^2 s_1 + e_0\mu^4 s_1 - 11e_0^4 + 2e_0^2\mu^2$$
$$- 3\mu^4))t^2 - 9e_0^2(e_0^2 + \mu^2)^6(e_0 s_1 - 3)x^2 + (6e_0^5\mu u_0(e_0^2 + \mu^2)^5 x^5 + 15e_0^4\mu u_0(e_0^2 + \mu^2)^5 x^4$$
$$+ 12e_0^3\mu u_0(3e_0^2 + \mu^2)(e_0^2 + \mu^2)^4 x^3 - 18e_0^2\mu u_0(e_0^2 + \mu^2)^4(e_0^3 s_1$$
$$+ e_0\mu^2 s_1 - 3e_0^2 - \mu^2)x^2 - 18e_0\mu u_0(e_0^2 + \mu^2)^4(e_0^3 s_1 + e_0\mu^2 s_1 + e_0^2 - 3\mu^2)x$$
$$- 9\mu u_0(e_0^2 + \mu^2)^4(6e_0^3 s_1 - 2e_0\mu^2 s_1 + e_0^2 - 3\mu^2))t + 9e_0(e_0^2 + \mu^2)^6(2e_0 s_1 + 3)x$$
$$+ 9(e_0^2 s_1^2 + e_0 s_1 + 1)(e_0^2 + \mu^2)^6].$$

Acknowledgment

References

References

[1] J.C. Eilbeck, J.D. Gibbon, P.J. Caudrey, R.K. Bullough, Solitons in nonlinear optics. I. A more accurate description of the 2π pulse in self-induced transparency, J. Phys. A: Math. Nucl. Gen. 6 (1973) 1337.

[2] A. Grauel, The Painlevé test, Bäcklund transformation and solutions of the reduced Maxwell-Bloch equations, J. Phys. A: Math. Gen. 19 (1986) 479-484.

[3] A. Grauel, Soliton connection of the reduced Maxwell-Bloch equations, Lett. Nuovo Cimento 41 (1984) 263-268.

[4] J.D. Gibbon, P.J. Caudrey, R.K. Bullough, J.C. Eilbeck, An N-soliton solution of a nonlinear optics equation derived by a general inverse method, Lett. Nuovo Cimento 8 (1973) 775-779.

[5] P.J. Caudrey, J.C. Eilbeck, J.D. Gibbon, Exact Multisoliton Solution of the Reduced Maxwell-Bloch Equations of Non-linear Optics, J. Inst. Math. Appl. 14 (1974) 375-386

[6] V.B. Matveev, M.A. Salle, Darboux Transformations and Solitons, Springer-Verlag, Berlin, Heidelberg, 1991.

[7] R. Guo, B. Tian, L. Wang, Soliton solutions for the reduced Maxwell-Bloch system in nonlinear optics via the N-fold Darboux transformation, Nonlinear Dyn. 69 (2012) 2009-2020.

[8] G.H. Shi, F. Fan, Properties of new soliton solutions on the non-vanishing background for the reduced Maxwell-Bloch system in nonlinear optics, Superlattice Microst. 101 (2017) 488-492.

[9] C. Garrett, J. Gemmrich, Rogue waves, Phys. Today 62 (2009) 62-63.

[10] N. Akhmediev, J.M. Dudley, D.R. Solli, S.K. Turitsyn, Recent progress in investigating optical rogue waves, J. Opt. 15 (2013) 060201.

[11] J.C. Chen, B. Li, Three-dimensional bright-dark soliton, bright soliton pairs, and rogue wave of coupled nonlinear Schrödinger equation with time-space modulation, Z. Naturforsch. 67 (2012) 483-490.

[12] Y.K. Liu, B. Li, Rogue waves in the (2+1)-dimensional nonlinear Schrödinger equation with a parity-time-symmetric potential, Chin. Phys. Lett. 34 (2017) 010202.

[13] D.H. Peregrine, J. Austral, Water waves, nonlinear Schrödinger equations and their solutions, Math. Soc. B: Appl. Math. 25 (1983) 16-43.

[14] N. Akhmediev, A. Ankiewicz, M. Taki, Waves that appear from nowhere and disappear without a trace, Phys. Lett. A 373 (2009) 675C678.

[15] F. Baronio, A. Degasperis, M. Conforti, S. Wabnitz, Solutions of the vector nonlinear Schrödinger equations: evidence for deterministic rogue waves, Phys. Rev. Lett. 109 (2012) 044102.

[16] C.Liu, Z.Y. Yang, L.C. Zhao, W.L. Yang, State transition induced by higher-order effects and background frequency, Phys. Rev. E 91 (2015) 022904.

[17] S.H. Chen, L.Y. Song, Rogue waves in coupled Hirota systems, Phys. Rev. E 87 (2013) 032910.

[18] E. Yomba, G.A. Zakeri, Rogue-pair and dark-bright-rogue waves of the coupled nonlinear Schrodinger equations from inhomogeneous femtosecond optical fibers, Chaos 26 (2016) 083115.

[19] F. Yuan, Y.S. Zhang, J.S. He, The rogue wave solutions of a new (2+1)-dimensional equation, Commun. Nonlinear Sci. Numer. Simulat. 30 (2016) 307-315.

[20] X. Wang, B. Yang, Y. Chen, Y.Q. Yang, Higher-order rogue wave solutions of the Kundu-Eckhaus equation, Phys. Scr. 89 (2014) 095210.

[21] X. Wang, Y.Q. Li, Y. Chen, Generalized Darboux transformation and localized waves in coupled Hirota equations, Wave Motion 51 (2014) 1149-1160.

[22] A. Chowdury, A. Ankiewicz, N. Akhmediev, Periodic and rational solutions of modified Korteweg-de Vries equation, Euro. Phys. J. D 70 (2016) 1-7.

[23] A.V. Slunyaev, E.N. Pelinovsky, Role of multiple soliton interactions in the generation of rogue waves: the modified Korteweg-de Vries framework, Phys. Rev. Lett. 117 (2016) 214501.

[24] Q.X. Xing, L.H. Wang, D. Mihalache, K. Porsezian, J.S. He, Construction of rational solutions of the real modified korteweg-de vries equation from its periodic solutions, arXiv:1704.05599v1 (2017).

[25] X.G. Geng, R.M. Li, Darboux transformation of the Drinfeld-Sokolov-Satsuma-Hirota system and exact solutions, Ann. Phys. 361 (2015) 215-225.

[26] P.S. Vinayagam, R. Radha, V.M. Vyas, K. Porsezian, Generalized gauge transformation approach to construct dark solitons of coupled nonlinear Schrödinger (NLS) type equations, Rom. Rep. Phys. 67 (2015) 737-751.

[27] M.S. Mani Rajan, Dynamics of optical soliton in a tapered erbium-doped fiber under periodic distributed amplification system, Nonlinear Dyn. 85 (2016) 599-606.

[28] U Saleem, M Hassan, Darboux transformation and exact multisolitons of CPN nonlinear sigma model, J. Math. Anal. Appl. 447 (2017) 1080-1101.

[29] B.L. Guo, L.M. Ling, Q.P. Liu, Nonlinear Schrödinger equation: generalized Darboux transformation and rogue wave solutions, Phys. Rev. E 85 (2012) 026607.

[30] L.H. Wang, K. Porsezian, J.S. He, Breather and rogue wave solutions of a generalized nonlinear Schrödinger equation, Phys. Rev. E 87 (2013) 053202.

[31] X. Wang, Y.Q. Li, F. Huang, Y. Chen, Rogue wave solutions of AB system Commun. Nonlinear Sci. Numer. Simul. 20 (2015) 434-442.

[32] S.H. Chen, D. Mihalache, Vector rogue waves in the Manakov system: diversity and compossibility, J. Phys. A: Math. Theor. 48 (2015) 215202.

[33] L. Wang, J.H. Zhang, C. Liu, M. Li, F.H. Qi, R. Guo, Breather-to-soliton transitions, nonlinear wave interactions, and modulational instability in a higher-order generalized nonlinear Schrödinger equation, Phys. Rev. E 93 (2016) 012214.

[34] L. Wang, J.H. Zhang, C. Liu, M. Li, F.H. Qi, Breather transition dynamics, Peregrine combs and walls, and modulation instability in a variable-coefficient nonlinear Schrödinger equation with higher-order effects, Phys. Rev. E 93 (2016) 062217.

[35] X. Wang, C. Liu, L. Wang, Darboux transformation and rogue wave solutions for the variable-coefficients coupled Hirota equations, J. Math. Anal. Appl. 449 (2017) 1534-1552.

[36] J.H. Zhang, L. Wang, Superregular breathers, characteristics of nonlinear stage of modulation instability induced by higher-order effects, Proc. R. Soc. A 473 (2017) 20160681.

[37] M.J. Ablowitz, D.J. Kaup, A.C. Newell, H. Segur, Nonlinear-evolution equations of physical significance, Phys. Rev, Lett. 31 (1973) 125.

[38] J. Wei, X.G. Geng, A hierarchy of new nonlinear evolution equations and generalized bi-Hamiltonian structures. Appl. Math. Comput. 268 (2015) 664-670.

[39] J. Wei, X.G. Geng, A vector generalization of Volterra type differential-difference equations. Appl. Math. Lett.55 (2016) 36-41.

[40] J. Wei, X.G. Geng, Quasi-periodic solutions to the hierarchy of four-component Toda lattices. J. Geom. Phys. 106 (2016) 26-41.

[41] R. Pal, H. Kaur, T.S. Raju, C.N. Kumar, Periodic and rational solutions of variable-coefficient modified Korteweg-de Vries equation, Nonlinear Dyn. 1 (2017) 1-6.
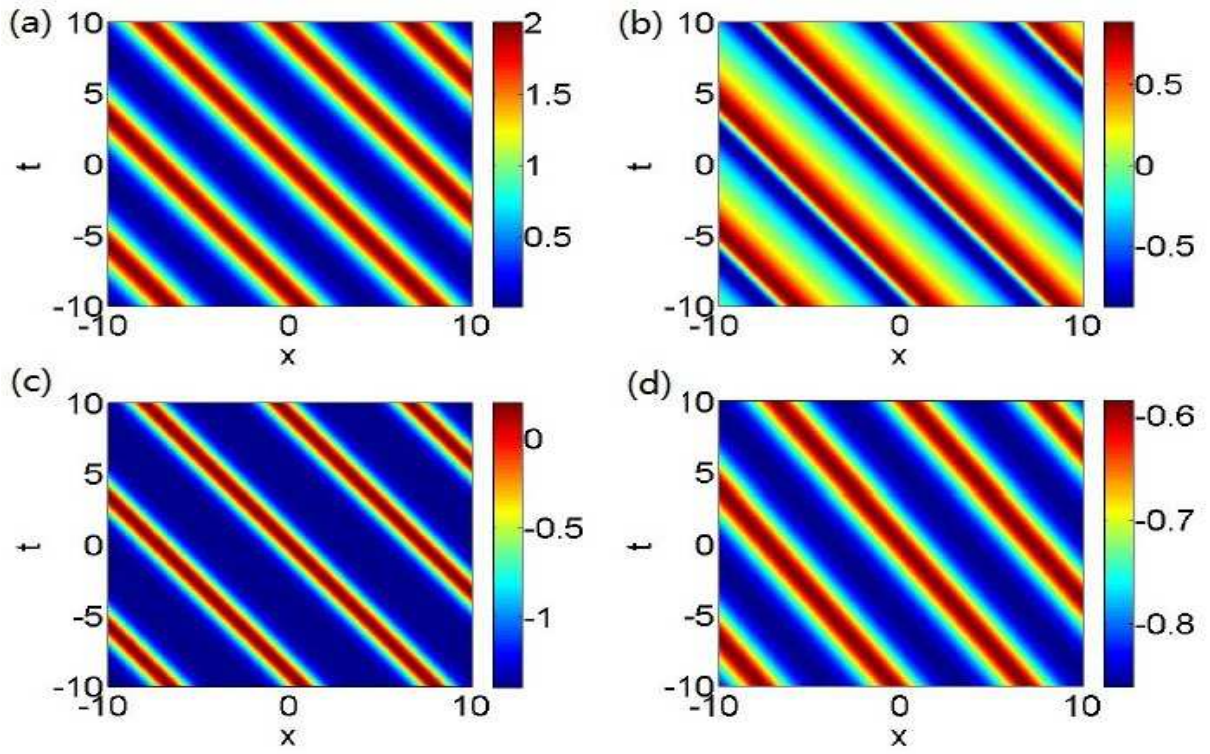
Fig. 1: (a)-(d) The first-order periodic solutions (10)-(12) for the components E, v, w with $\mu = 1$ and (13) for the component u with $\mu = 0.2$. The other parameters are $e_0 = 1, u_0 = 1, \kappa_1 = 0.5$.
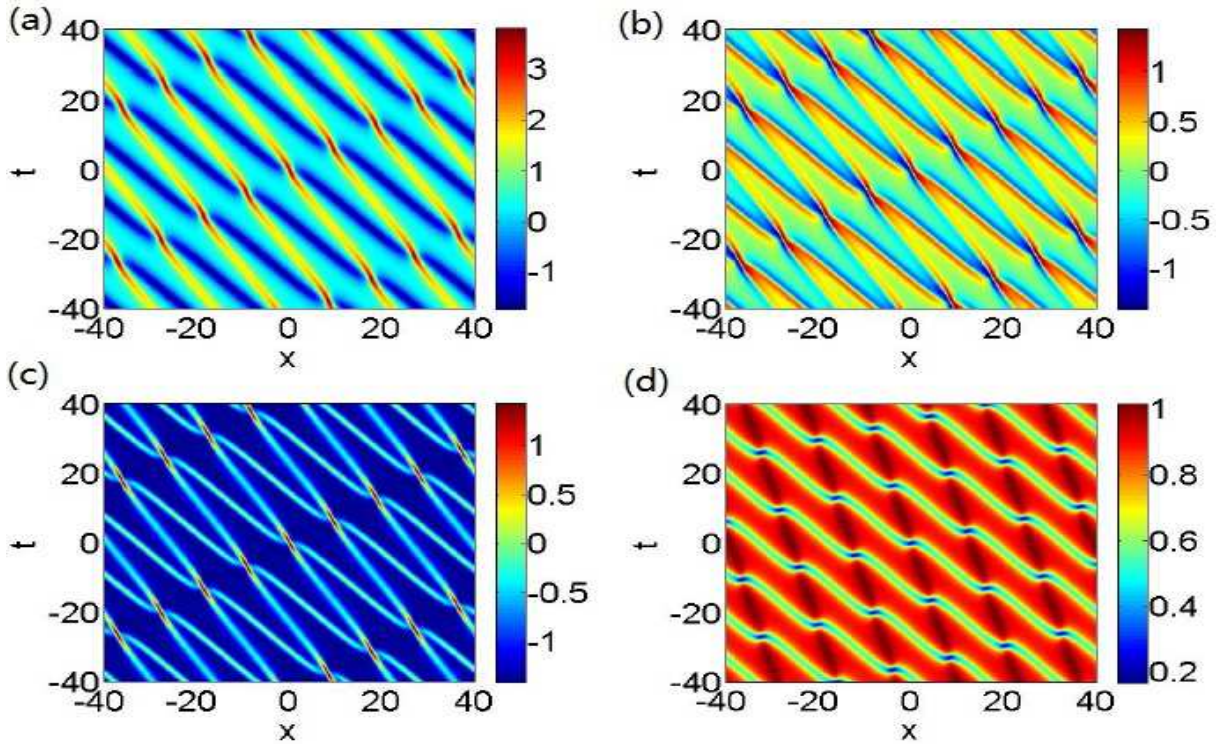
Fig. 2: (a)-(d) The second-order periodic solutions (14)-(16) for the components E, v, w with $\mu = 1$ and (17) for the component u with $\mu = 0.2$. The other parameters are $e_0 = 1, u_0 = 1, \kappa_1 = 0.5, \kappa_2 = 0.25$.
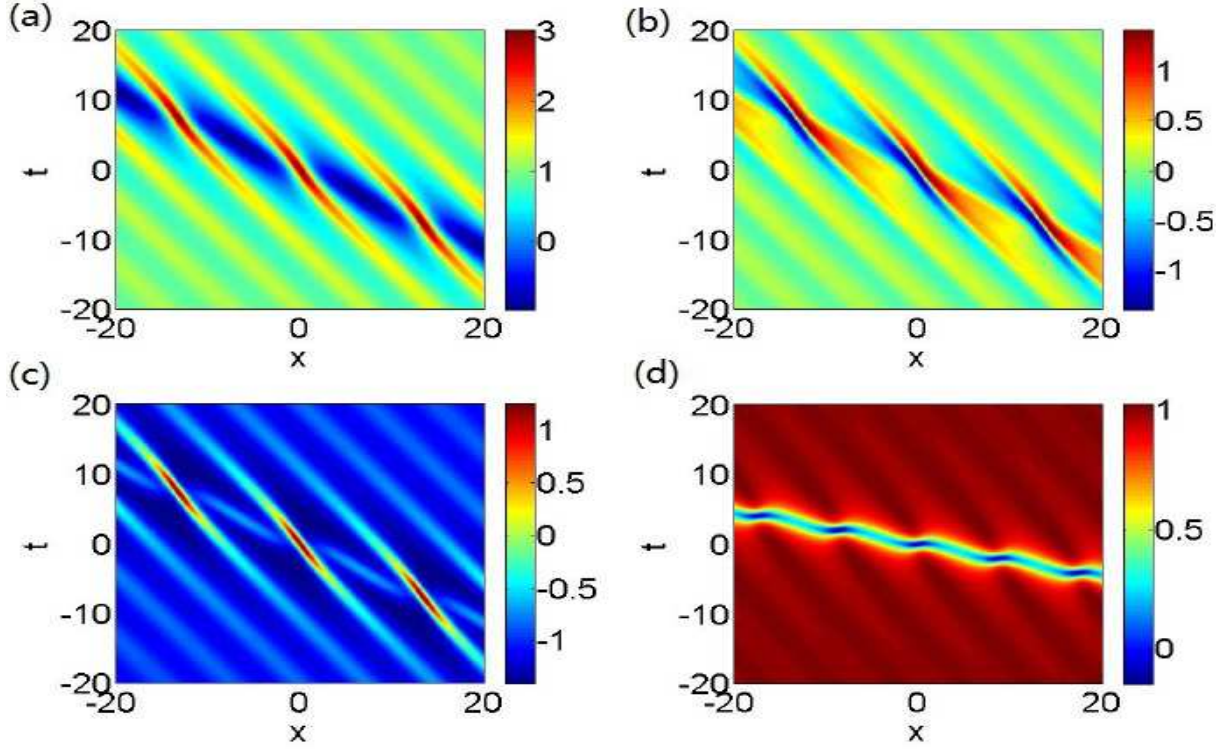
Fig. 3: (a)-(d) The degenerate periodic solutions (24)-(26) for the components E, v, w with $\mu = 1$ and (27) for the component u with $\mu = 0.2$. The other parameters are $e_0 = 1, u_0 = 1$.
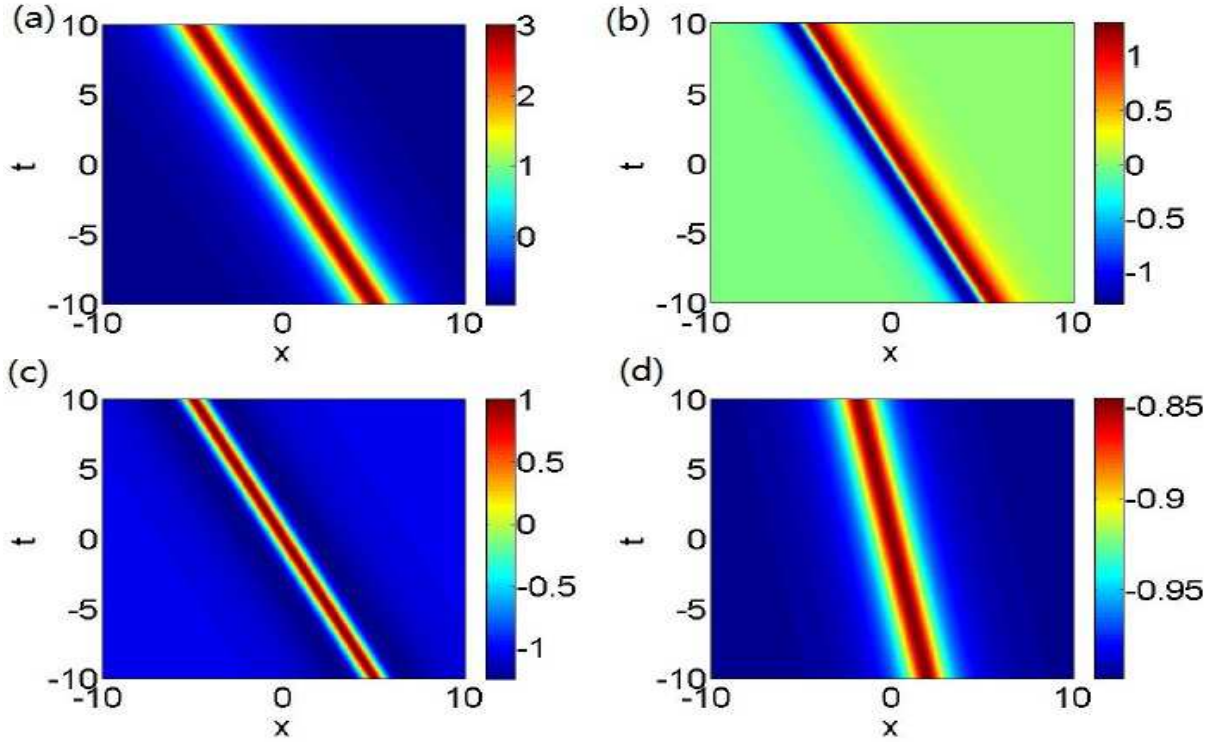
Fig. 4: (a)-(d) The first-order rational solutions (34)-(36) for the components E, v, w with $\mu = 1$ and (37) for the component u with $\mu = 0.2$. The other parameters are $e_0 = 1, u_0 = 1$.
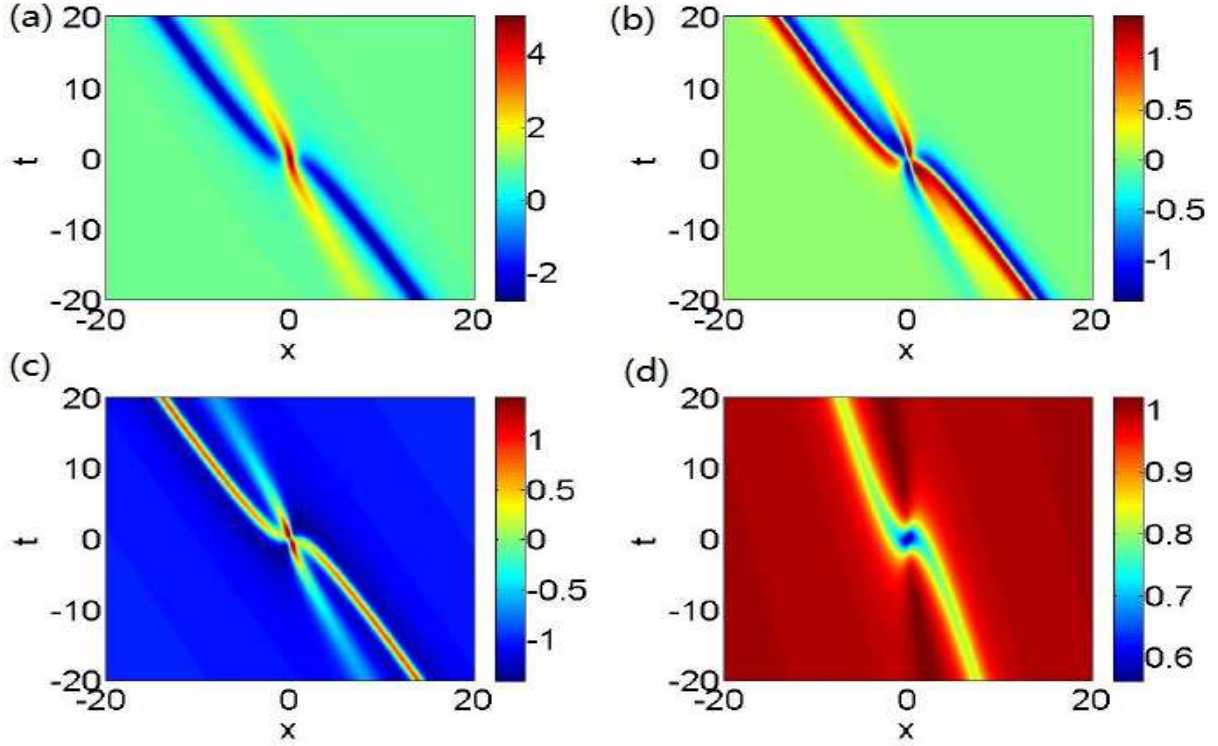
Fig. 5: (a)-(d) The second-order rational solutions (39)-(41) for the components E, v, w with $\mu = 1$ and (42) for the component u with $\mu = 0.2$. The other parameters are $e_0 = 1, u_0 = 1, s_1 = 0$.
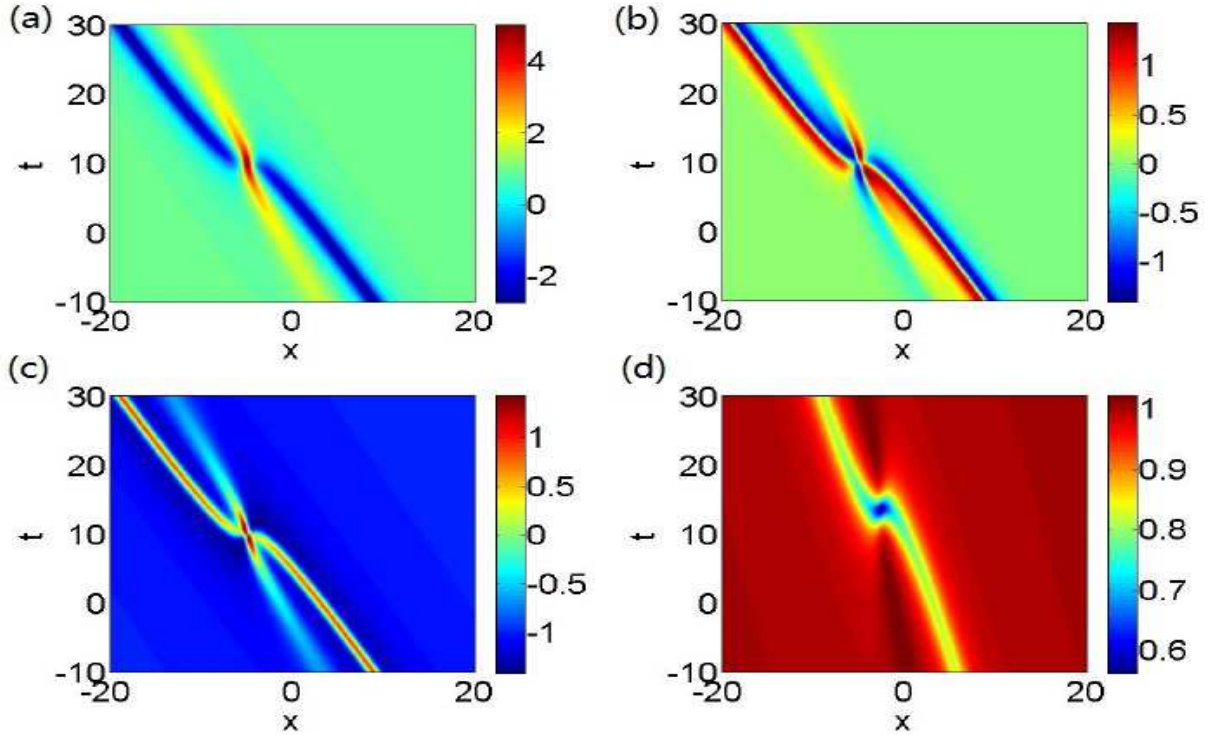
Fig. 6: (a)-(d) The second-order rational solutions (39)-(41) for the components E, v, w with $\mu = 1$ and (42) for the component u with $\mu = 0.2$. The other parameters are $e_0 = 1, u_0 = 1, s_1 = 10$.

16
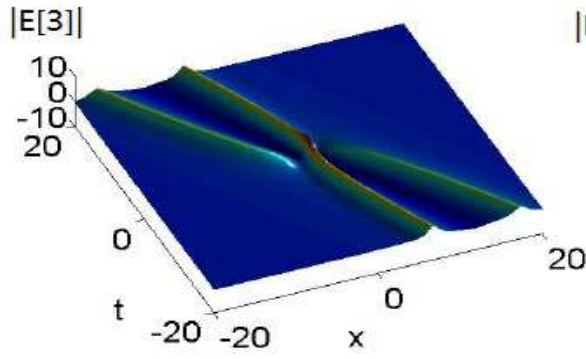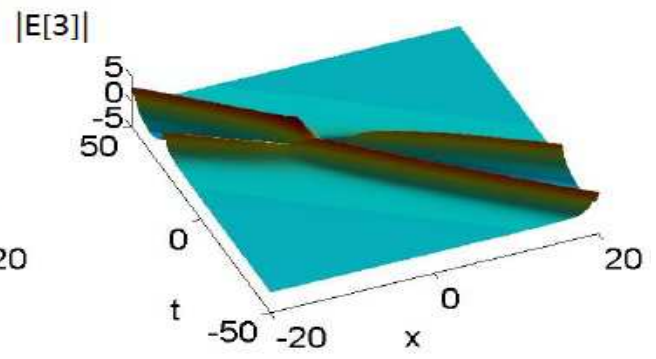
Fig. 7: (a),(b) The third-order rational solutions for the component E with $s_1 = 0$ and $s_1 = 10$. The other parameters are $e_0 = 1, \mu = 1, u_0 = 1, s_2 = 0$.
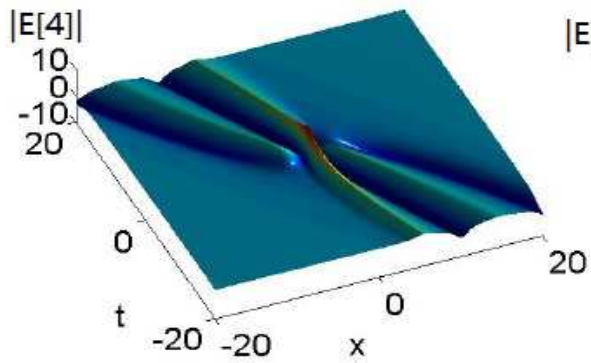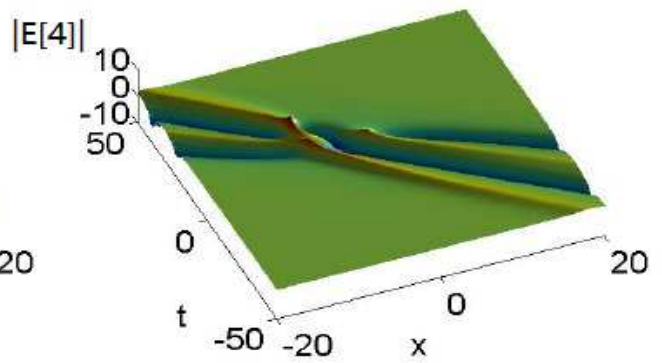
Fig. 8: (a),(b) The fourth-order rational solutions for the component E with $s_1 = 0$ and $s_1 = 10$. The other parameters are $e_0 = 1, \mu = 1, u_0 = 1, s_2 = s_3 = 0$.